Journal of Crystal Growth 123 (1992) 75–94
North-Holland

JOURNAL OF CRYSTAL GROWTH

Fabrication and properties of epitaxially stabilized Ge/α-Sn heterostructures on Ge(001)

W. Wegscheider [1]
Walter Schottky Institut, Technische Universität München, D-W-8046 Garching, Germany

J. Olajos
Department of Solid State Physics, University of Lund, S-221 00 Lund, Sweden

U. Menczigar, W. Dondl and G. Abstreiter
Walter Schottky Institut, Technische Universität München, D-W-8046 Garching, Germany

Received 29 April 1992

We have investigated the influence of the growth parameters during molecular beam epitaxy on the realizibility of diamond crystal structure Ge/α-Sn alloys and superlattices on Ge(001) substrates. The segregation behaviour of Sn during Ge overgrowth has been studied. We find that for growth temperatures higher than 300°C the incorporation rates are less than 0.005 ML^{-1}. The low-energy electron diffraction data of a series of $Ge_{0.9}Sn_{0.1}$ films deposited at substrate temperatures in the range of 185 to 275°C indicate a transition to amorphous growth for thicknesses beyond 20 Å. Single-crystal Ge_nSn_m superlattices with α-Sn layer thicknesses m of 1 and 2 monolayers and periodicities $n+m$ between 10 and 22 monolayers have been fabricated by an unconventional molecular beam epitaxy technique which involves large substrate temperature modulations during growth. Structural characterization of the samples by means of transmission electron microscopy, Raman spectroscopy and X-ray diffraction exhibits distinct superlattice effects. The downward shift of the fundamental energy gap of the superlattices with increasing Sn content, as extracted from absorption measurents with a Fourier transform spectrometer, is in excellent agreement with theoretical values obtained from pseudopotential band structure calculations. The films were found to be stable against phase transition up to temperatures of 430–465°C, depending on the average Sn content.

1. Introduction

One of the most fascinating ideas in modern semiconductor physics represents the realization of a direct energy-gap material based on group IV elements. Stimulated by the development of growth techniques such as molecular beam epitaxy (MBE) during the past few years which allow precise control of layer thicknesses on an atomic scale most of the experimental work in order to achieve this goal concentrates on the synthesis of short-period Si/Ge superlattices (SLs). As predicted by Gnutzmann and Clausecker [1] in 1974, these structures should possess a quasidirect band-gap which originates from artificially breaking the cubic symmetry of the constituent elements and folding back the lowest conduction band state into the Γ point. Although there exists experimental evidence for new optical transitions obtained from electroreflectance [2] and photoluminescence measurements [3] which support this concept the optical oscillator strengths of such SLs with appropriate layer thicknesses and strain situations are expected to be very small compared

[1] Present address: Room 1C-417, AT&T Bell Laboratories, 600 Mountain Avenue, Murray Hill, New Jersey 07974, USA.

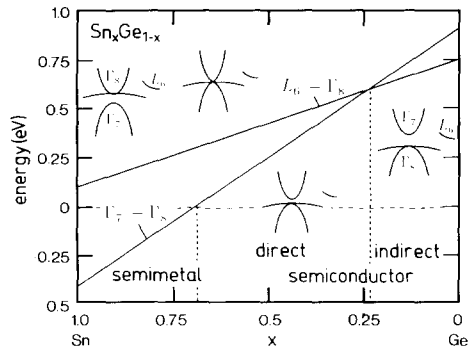

Fig. 1. Linear interpolation of the energy differences $\Gamma_7 - \Gamma_8$ and $L_6 - \Gamma_8$ between the bulk band structures of α – Sn and Ge. The arrangement of the relevant bands for a series of hypothetical $Ge_{1-x}Sn_x$ alloys is also indicated.

to intrinsically direct energy-gap semiconductors like GaAs (see, for example, refs. [4–6]).

1.1. Band structure of $Ge_{1-x}Sn_x$ alloys

On the other hand as visualized in fig. 1 by a simple linear interpolation between the bulk band structures of α-Sn and Ge, alloying of Ge with Sn should yield a material with a fundamental direct energy-gap for Sn contents in the range of about 20% to 70%. This is a consequence of the unusual band ordering at $\boldsymbol{k} = (0, 0, 0)$ of the diamond structure semimetallic α-Sn phase (grey tin) as was established by Groves and Paul [7] in 1963. In α-Sn, the large interaction between the overlapping Γ_7^- and Γ_8^+ bands which form the direct gap in Ge leads to an inversion of the curvature of these bands in comparison to the other group IV semiconductors. In this way, the "light hole" Γ_8^+ band transforms into a conduction band, whereas the Γ_7^- states which are located about 0.3 eV below the valence band edge become a filled valence band. Because the Γ_8^+ conduction band has to be degenerate with the heavy hole band of the same symmetry at the Γ point, α-Sn is sometimes referred to as a symmetry induced zero-gap semiconductor.

Although the assumption that the energetic positions at the critical points of the band structure vary linearly with composition lacks justification, the three band-gap types "semimetallic, direct and indirect" which appear in fig. 1 are also expected from ab initio pseudopotential [8] and tight-binding calculations in the virtual crystal approximation (VCA) [9]. However, the "direct gap windows" predicted by these authors ($0.2 < x < 0.6$ and $0.26 < x < 0.74$, respectively) differ slightly from that indicated in fig. 1.

The possibility of obtaining a semiconductor with a direct band-gap adjustable from ≈ 0.5 eV to zero by growth of $Ge_{1-x}Sn_x$ alloys with an appropriate Sn content x offers the potential for the fabrication of long-wavelength detectors and light emitting devices which have so far predominantly been made of III/V and II/VI compound semiconductors. Furthermore, as already pointed out by Goodman [10] in 1982, such structures should show very high carrier mobilities due to the absence of polar scattering. In addition, the large difference in the electron mobilities at the Brillouin zone centre and at the L-point [$\boldsymbol{k} = (1, 1, 1)$] as sketched in fig. 1 should be favourable for observing the Gunn effect associated with an electron transfer from the high-mobility region in $\boldsymbol{k}$-space to the low-mobility region [8]. Especially interesting would be the situation when the Γ_7^- minimum just touches the Γ_8^+ valence band ($x \approx 0.7$) since in this case both bands would show infinitely small effective masses due to their infinitely high curvature at $\boldsymbol{k} = (0, 0, 0)$ [8,10].

1.2. Problems in $Ge_{1-x}Sn_x$ crystal growth

It is well known that bulk tin undergoes a phase transition from the diamond structure α phase to the metallic body centred β phase when a temperature of 13.2°C is exceeded [11]. However, Ewald [12] reported already in 1954 on a distinct increase of this transition temperature of single-crystalline α-Sn samples containing 0.75 wt% Ge to values above 60°C. A further increase to 70°C was observed when it was possible to prepare epitaxial α-Sn films on the closely lattice matched InSb and CdTe substrates by MBE nearly 30 years later [13]. The highest transition temperatures of epitaxially stabilized α-Sn which have been achieved so far with these substrate materials are about 130°C [14,15]. Analogously, the stability of $Ge_{1-x}Sn_x$ alloys should be criti-

cally dependent on their epitaxial registry on a diamond structure substrate material.

Most of the growth of such substrate-stabilized alloys has been attempted on [001] oriented CdTe, InSb and Ge. A recent overview of these efforts has been given by Fitzgerald et al. [16]. Although relatively thick Sn-rich alloys ($x > 0.9$) pseudomorphic to the two former substrate materials with excellent crystallinity have been reported [17], the use of Ge as substrate is preferred from the technological point of view. Since the lateral lattice constant of Ge can be also obtained by growth of thick fully relaxed $Si_{1-x}Ge_x$ layers continuously graded from $x = 0$ to 1 on Si(001) substrates [18,19], this would offer in principle the potential for the integration of Ge/α-Sn heterostructures with the highly developed Si technology.

One of the major problems in the fabrication of single-crystal Ge/α-Sn heterostructures, however, is the large difference in the intrinsic lattice constants of Ge ($a = 5.658$ Å) and α-Sn ($a = 6.489$ Å). This results in a misfit f, defined by $(a_s - a_f)/a_f$ (a_s and a_f denote the bulk lattice constants of substrate and film material) of -12.8% for pseudomorphic growth of a $\alpha - Sn$ layer on Ge substrate. In comparison, a Ge film pseudomorphic to a Si substrate has to be laterally compressed by only -4%. Assuming Vegard's law, which means that the relaxed lattice constant of $Ge_{1-x}Sn_x$ can be calculated by linear interpolation between the lattice constants of α-Sn and Ge, a lattice mismatch of about -3% is obtained for an alloy with only 20% Sn content pseudomorphic to Ge. Taking this value into account, the maximum critical thickness for coherent growth of such structures ($x > 0.2$) according to the equilibrium theory after Frank and Van der Merwe [20] and Matthews and Blakeslee [21] is expected to be less than 25 Å (see appendix). Provided that the onset of relaxation is retarded, as in the case of strained Si/Ge heterostructures, metastable unrelaxed $Ge_{0.8}Sn_{0.2}$ films on Ge should not exist for thicknesses above about 30 Å [22]. This is confirmed by Gossmann [23], who has studied the growth morphology of such layers on Ge(001) by in situ reflection high-energy electron diffraction (RHEED) and finds that two-dimensional growth only occurs for film thicknesses less than 5–30 Å for $1 > x > 0.2$.

Unfortunately, two further difficulties have to be overcome before high-quality $Ge_{1-x}Sn_x$ alloys with the desired properties, i.e. a tunable bandgap between 0.7 eV and zero, can be synthesized. Firstly, in contrast to the Si/Ge system, which is completely miscible, the solid solubility of Sn in Ge is limited to about 1%. Secondly, Sn has a pronounced tendency to segregate on the surface of the growing $Ge_{1-x}Sn_x$ film even at substrate temperatures as low as $T_s = 150$°C [24]. These problems emphasize the necessity to realize growth conditions for $Ge_{1-x}Sn_x$/Ge(001) structures far away from thermodynamic equilibrium which are not practically achievable with conventional MBE systems. It is therefore not surprising that, to our knowledge, experimental evidence of a material with and fundamental energy gap below that of Ge has only be reported for Ge/α-Sn heterostructures which have been prepared by a novel growth technique [25–27].

In this paper we report on the limitations in structural design of Ge/α-Sn heterostructures which can be prepared by MBE on Ge(001) substrates. We concentrate on short-period Ge/α-Sn SLs and compare the optical properties of these structures with theoretical predictions obtained from band-structure calculations. The paper is organized in the following way: in section 2 the experimental details of the growth apperatus, as well as of the characterization intstruments are outlined; section 3 first describes the incorporation behaviour of Sn during Ge growth, which turns out to play a crucial role with regard to the realizibility of alloys and SLs based on these two elements (subsections 3.2 and 3.3) and then discusses the optical properties and the structural stability of the latter structures; section 4 contains conclusions and prospects in view of future requirements which could enlarge the range of achievable Ge/α-Sn heterostructures.

2. Experimental techniques

All of the samples for this study were deposited on [001] oriented Ge substrates (50 Ω

cm) using a custom-built MBE system equipped with in situ low-energy electron diffraction (LEED) and Auger electron spectroscopy (AES) surface analysis instruments. Prior to the Ge/α-Sn heterostructure growth, a Ge buffer layer with a thickness of about 200 Å has been deposited following a special temperature profile, which involves coverage of the substrate with about 10 Å at $T_s = 200$°C and subsequent ramping up the substrate temperature to 450°C. This procedure is necessary, due to the volatility of the oxides formed by Ge which prevents in contrast to Si [28] sufficient protection of the Ge surface by a passivating chemical oxide layer. However, it allows to cover residual carbon contamination on the order of a few percent of an atomic monolayer (ML) of the starting surface which are still present after chemical precleaning and in situ oxide removal by thermal desorption at $T_s = 720$°C for 10 min. In addition, the Ge buffer provides the clean and planar surface required for defect-free, epitaxial growth of the subsequent layers [29]. Ge and Sn were both evaporated from conventional Knudsen-type effusion cells using pyrolytic boron nitride (PBN) crucibles. Typical temperatures of 1140 and 880°C for the Ge and Sn ovens, respectively, lead to growth rates of about 5 Å/min at a background pressure in the upper 10^{-11} mbar (base pressure $< 3 \times 10^{-11}$ mbar) range. The growth rates were calibrated with a quartz crystal microbalance. The substrate holder is in thermal contact with a cooling tank through which liquid nitrogen is passed. In combination with a tantalum heater which is directly located behind the substrate, this allows rapid temperature variations. The substrate temperature during growth was controlled via a thermocouple which was previously calibrated with either a pyrometer ($450 < T_s < 900$°C) or by pressing another thermocouple onto the sample surface.

Cross-sectional transmission electron microscopy (TEM) specimens were prepared in ⟨110⟩ orientation. Bright field, lattice imaging, and selected area electron diffraction (SAD) were performed in a JEOL 200CX microscope equipped with a high-resolution side entry goniometer offering a point-to-point resolution of about 2.8 Å. Raman spectroscopical measurements were carried out in $001(110/110)00\bar{1}$ backscattering geometry at 77 K using the 568.2 nm line of a Kr^+ laser and a conventional Raman set-up with triple grating spectrometer equipped with a photo-diode multichannel detector. X-ray spectra were measured using Cu Kα radiation and a double crystal diffractometer. The infrared absorption measurements were performed on a BOMEM DA3.02 Fourier transform infrared (FTIR) spectrometer equipped with a LN_2-cooled InSb photodetector and a continuous-flow cryostat.

3. Results and discussion

3.1. Sn segregation

In order to investigate the segregation behaviour of Sn on Ge(001) during MBE at low substrate temperatures, the following experiment was performed. A Sn adlayer of 3.12×10^{14} atoms/cm^2 which corresponds to 0.5 ML was deposited at $T_s = 270$°C and the intensity I_0 of the Sn(430 eV) Auger line was recorded. This layer was then overgrown by 100 ML of pure Ge at a constant substrate temperature which was varied from room temperature to 460°C. Simultaniously the Sn AES intensity was monitored in intervals ranging from 5 to 20 ML. It should be mentioned at this point that re-evaporation of Sn can be neglected within the whole range of T_s used in this study, since no change of the Sn AES intensity could be observed, even when a growth interruption of several hours at $T_s = 460$°C was introduced before Ge deposition took place. Fig. 2 shows the Sn Auger intensity normalized to the initial intensity I_0 as a function of the Ge coverage for selected substrate temperatures. The broken line which coincides very well with the experimental values for room temperature deposition and also for growth at 77°C reflects the expected Sn AES intensity decrease for an ideal heterostructure, i.e. for an atomically abrupt interface between the Sn and Ge layer without Sn segregation. In order to determine the amount of Sn which segregates on the Ge surface from

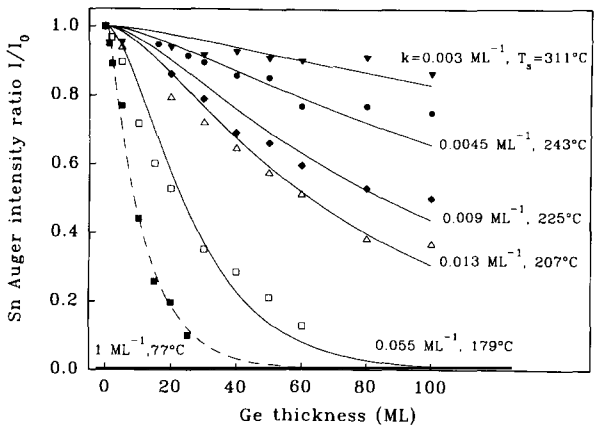

Fig. 2. Auger intensity of a 0.5 ML thick Sn layer (430 eV line) on Ge(001) as a function of Ge coverage for different substrate temperatures T_s normalized to its initial value. The lines represent the calculated intensity decay for various incorporation rates k.

Auger data, we assume that for a given substrate temperature, a constant rate k of the Sn atoms within the adlayer incorporate into the growing Ge film. An analogous model has been previously applied by Iyer et al. for studying dopant incorporation in Si [30] and recently by Wilhelm et al., who investigated the segregation behaviour of Sb during Ge epitaxy [31]. The solid lines in fig. 2 correspond to the calculated Sn AES intensities. Best agreement with the measured values was obtained for the incorporation rates k indicated in fig. 2. The strong decrease of the incorporation rate with increasing substrate temperature demonstrates the pronounced tendency of Sn to segregate on the Ge surface. Even at a temperature as low as 179°C, only about 6% of the Sn atoms are incorporated into each growing Ge monolayer.

In addition to these AES investigations on the segregation behaviour of Sn, LEED was applied to judge the crystalline quality of the films. In the temperature window of about 310 to 400°C, we obtain sharp diffraction spots after 100 ML Ge overgrowth. Similar to previous studies of the growth morphology during Ge homoepitaxy [32], a distinct broadening of the LEED spots related to an enhancement of the surface roughness can be detected with increasing Ge coverage at substrate temperatures below 310°C. An increase of the substrate temperature to values above 400°C, however, is accompanied by the occurrence of additional spots in the LEED pattern characteristic for island formation and facetting. In contrast to the samples grown at $T_s < 400$°C, the surface of these samples is no longer mirror-like. Optical inspection under a microscope exhibits the formation of small droplets which may be due to Sn precipitation and subsequent phase transformation.

3.2. $Ge_{1-x}Sn_x$ alloys

The usual method of growing an alloy layer by means of MBE is to adjust the appropriate flux rates in order to achieve the desired composition and then to allow both materials to arrive on the sample surface simultaneously. Provided that the simple model of a constant Sn incorporation rate from an adlayer also holds for growth of $Ge_{1-x}Sn_x$ alloys, initially only a fraction k of the nominal Sn concentration x is incorporated in the layers and a surface reservoir builds up. Since this model assumes that the driving force for incorporation increases as more and more Sn accumulates on the surface, the Sn content of the alloy layer finally approaches its nominal value. The equilibrium adlayer thickness in monolayers at which the Sn incorporation rate equals its arrival rate is given by x/k. The resulting concentration profile for a 350 ML thick alloy with $x = 0.1$ and an incorporation rate of about 0.06 ML^{-1}, which corresponds to a substrate temperature of about 180°C (see fig. 2), is depicted in fig. 3. The nominal Sn concentration of 10% is reached at an alloy layer thickness of about 60 ML. The amount of Sn which rides on the surface at this coverage is approximately 1.7 ML. As deposition continues this Sn adlayer thickness remains constant and Sn concentrations of 1.0 and 0.7 are obtained in the topmost (350th ML) and subsurface monolayer (349th ML), respectively (fig. 3). In the inset of this figure the expected decay of the Auger intensity ratio I_{Ge}(47 eV)/I_{Sn}(430 eV) of such a structure (solid line) is compared with that of an alloy with a constant Sn content of 10% throughout the whole layer (dashed line).

It is obvious that high-quality $Ge_{1-x}Sn_x$ crystal growth can only be expected for an adlayer thickness which is less than the critical thickness of pure α-Sn on Ge(001). The latter has been determined to be of the order of 3–4 ML. At this thickness the intensity of the LEED reflections from α-Sn layers deposited at different substrate temperatures ($20 < T_s < 130$°C) drastically decreases.

In combination with the results given in the previous subsection, these considerations emphasize the necessity to lower the substrate temperature to values well below 310°C in order to meet the condition $x/k < 4$ ML for alloy compositions exceeding the solid solubility limit ($x \approx 0.01$). For this reason the substrate temperatures for deposition of a series of $Ge_{0.9}Sn_{0.1}$ films of $T_s = 185$, 225 and 275°C have been chosen. The Auger intensity ratios I_{Ge}/I_{Sn} recorded during growth of the sample at $T_s = 185$°C have been included in the inset of fig. 3. These data exemplary demonstrate that the concentration profile which one would expect for this substrate temperature from the growth model has been indeed achieved. Fig. 4 shows the LEED intensity profiles which

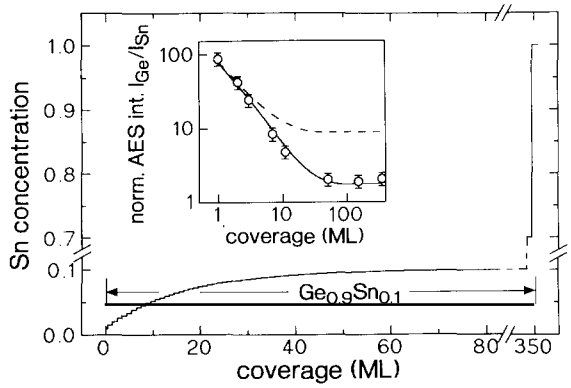

Fig. 3. Calculated distribution of Sn within a nominal $Ge_{0.9}Sn_{0.1}$ alloy layer of 350 ML thickness. The underlying growth model assumes a constant incorporation rate of 0.06 ML^{-1} from a Sn surface adlayer whose equilibrium thickness after growth of about 60 ML is close to 1.7 ML. The inset shows the intensity ratio of the Ge(47 eV) to the Sn(430 eV) Auger line normalized to their bulk intensities as a function of coverage for the calculated concentration profile (solid line) and the nominal structure (dashed line). The experimental data points have been obtained during deposition of a corresponding structure at $T_s = 185$°C.

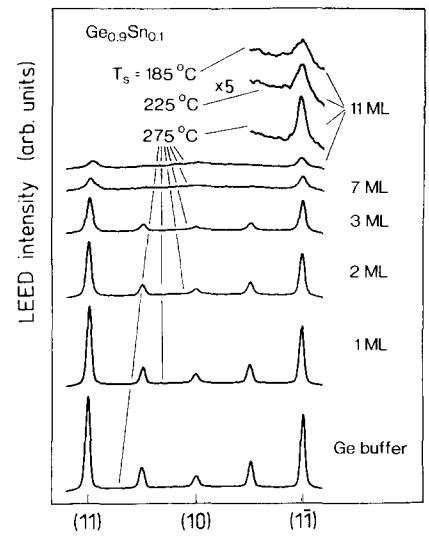

Fig. 4. LEED intensity profiles ($E_e = 44$ eV) recorded during deposition of $Ge_{0.9}Sn_{0.1}$ alloy layers. The substrate temperatures T_s are indicated.

were recorded during growth of the first monolayers of these structures. With increasing alloy thickness, a continuous decrease of the spot intensities is observable, indicating a transition to amorphous growth. A comparison of the intensity profiles of the three samples after growth of 11 ML clearly shows that this loss of crystalline order is further accelerated when reducing the substrate temperature from 275 to 185°C. Successful synthesis of $Ge_{1-x}Sn_x$ films can therefore be excluded for even lower substrate temperatures.

From these results we conclude that the requirements on the growth parameters for single-crystal alloy layers with $x \geq 0.1$ on Ge(001) substrates are not compatible with conventional MBE. Further investigations should therefore concentrate on the effect of structural modifications, e.g. modulated layer sequences as well as on growth methods which support depostition far away from thermodynamic equilibrium.

3.3. Ge / α-Sn superlattices

The idea to fabricate Ge/α-Sn superlattices instead of alloy layers is to overcome the problem

of Sn segregation at typical substrate temperatures for crystalline Ge growth by adjusting different growth parameters for the two material species. Since high-quality Ge deposition demands substrate temperatures on the order of 300°C, and substantial Sn incorporation occurs only below 100°C, it is essential to modulate T_s over a wide range within one superlattice period.

3.3.1. Structural characterization

In order to optimize the substrate temperature profile during growth of superlattices based on Ge and Sn, a set of samples each consisting of an alternating sequence of 2 ML Sn and 20 ML Ge ($Ge_{20}Sn_2$) has been prepared. Fig. 5 compares the I_{Sn}/I_{Ge} AES intensity ratios recorded within the first period of such structures deposited at different substrate temperatures. Whereas the increase of I_{Sn}/I_{Ge} during growth of the Sn layer is almost identical for the three samples, the AES

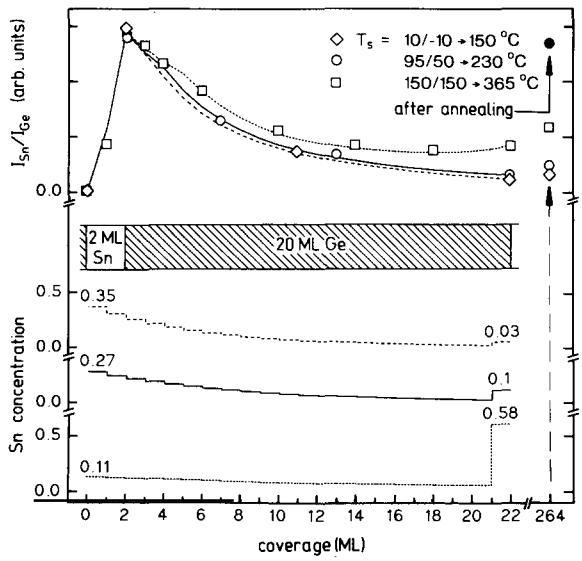

Fig. 5. Ratio of the AES intensities of the Sn(430 eV) and the Ge(47 eV) line as a function of coverage in the first, and after completion of the 12th, period of $Ge_{20}Sn_2$ SLs grown at different temperatures. The first indicated substrate temperatures correspond to Sn growth, the second temperatures which were changed from the lower to the higher value to Ge growth. Best fit to experimental data is obtained for the given Sn concentration profiles. The increase of the I_{Sn}/I_{Ge} signal due to annealing of an amorphous $Ge_{20}Sn_2$ SL ($T_s = -26$°C) for 10 min at 500°C is indicated by the filled circle.

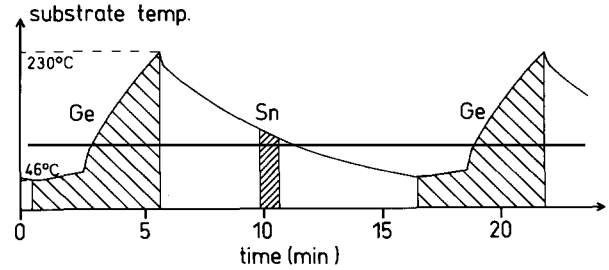

Fig. 6. Variation of T_s during growth of a $Ge_{20}Sn_2$ SL. The hatched regions mark the times when either the Ge or the Sn shutter was open.

ratios for different substrate temperature profiles diverge with increasing Ge coverage. It is important to note that Sn growth took place at the first temperature value indicated in fig. 5, whereas T_s was kept almost constant at the lower value of the given temperature interval for the first 8 ML of Ge deposition. Subsequently, the substrate temperature was increased to the higher value. A typical temperature profile is shown in fig. 6 for the case of $T_s = 95/50$–230°C. As a reference for the AES analysis, we have also deposited an equivalent structure at a constant temperature of −26°C where diffusion and segregation effects are negligible. Comparison of the AES signals with those measured during growth of the reference sample reveals that independent of the temperature for Sn deposition ($-26 < T_s < 150$°C), sharp Ge/Sn interfaces are obtained. In contrast, segregation plays a crucial role when Ge overgrowth takes place as can be seen from the Sn concentration profiles depicted in the bottom part of fig. 5. The latter have been calculated by employing the Sn incorporation model already discussed in subsection 3.1 with the exception that the incorporation rate k was allowed to decrease with increasing Ge coverage in order to take the rise of T_s into account. For the superlattice structures deposited in the substrate temperature intervals of $-10 < T_s < 150$°C and $50 < T_s < 230$°C, best fit to experimental data is obtained for a Sn content of 3% and 10%, respectively, in the topmost layer, which corresponds to at least 95% incorporation within one superlattice period. As the substrate temperatures are further increased to $150 < T_s < 365$°C, a Sn adlayer of

more than half a monolayer remains on the surface after completion of the first period. Examination of the Auger data of this sample shows that the I_{Sn}/I_{Ge} ratio for a coverage of 22 ML exceeds that recorded at 18 ML. In this case, the strong increase of the substrate temperature at the end of the period leads obviously to a transfer of Sn from deeper layers onto the surface, since there has been no Sn deposition in between these measurements. From a comparison of the Auger data of the three samples after completion of the first and the 12th period (marked by an arrow in fig. 5), we furthermore conclude that for the SLs deposited at maximum substrate temperatures of 150 and 230°C, no appreciable Sn transfer occurs beyond one period. However, for the sample grown at the highest temperatures ($150 < T_s < 365$°C), an accumulation of more than 1 ML is observable after 12 periods.

Analogous to the characterization of the alloy layers described in the previous subsection, in addition to the AES measurements LEED analysis was performed during deposition of the SLs in order to obtain information on the crystallinity of the films. Fig. 7 shows the evolution of diffracted electron intensity ($E_e = 182$ eV) from the surfaces of the three samples with increasing superlattice period. Although a maximum substrate temperature of 150°C is too high to inhibit Sn segregation, the distinct decrease of the LEED intensity already after the second superlattice period clearly demonstrates that this low temperature is not sufficient to preserve crystalline growth. In contrast, for the SL grown at the next highest temperature interval ($50 < T_s < 230$°C), the initial LEED intensities are maintained after the 12th and also after the 20th period (not shown). However, a further increase of T_s to a maximum value of 365°C is accompanied by surface roughening, as can been seen from the broadening and the decay in intensity of the corresponding LEED spots in fig. 7. It is remarkable that a substantial decrease of the LEED intensities only occurs at the beginning of the second period of this sample whereas all profiles recorded during subsequent growth are almost identical. This gives strong indication that the critical thickness for pseudomorphic Sn growth

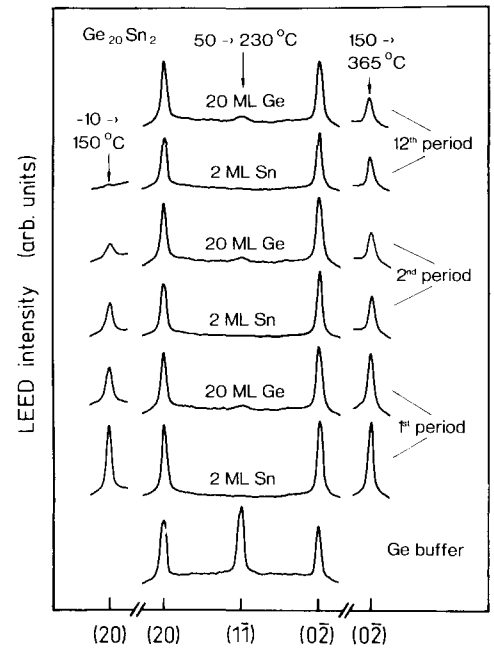

Fig. 7. LEED intensity profiles ($E_e = 182$ eV) recorded during deposition of $Ge_{20}Sn_2$ SLs. The indicated temperature intervals correspond to the variations of T_s within the Ge layers of the different samples.

on Ge has already been exceeded when depositing the Sn layer of the second period. This may be understood when we consider the enlargement of the thickness of this layer to about 2.6 ML, due to Sn segregation out of the first superlattice period. The concept of adjusting different growth conditions for Ge and Sn to achieve compositional modulations while crystallinity is maintained seems, however, to work also for this sample. The LEED intensity profiles shown in fig. 8 which have been recorded within the first superlattice period reveal that although coverage of Sn with Ge at low substrate temperatures results in a loss of crystalline order, the initial crystal quality can be almost completely regained by ramping up T_s. A related technique called solid phase epitaxy has already been used to successfully fabricate Sb δ-doping layers in Si MBE [33]. In this case the doping material which shows a very similar segregation behaviour is covered by an amorphous Si layer deposited at room temperature. Sharp doping profiles are then achieved by recrystallization

of the amorphous layer at a substrate temperature of 700°C. In order to verify the applicability of this method also to Ge/α-Sn heterostructures, we performed the following experiment. After covering the amorphous $Ge_{20}Sn_2$ SL ($T_s = -26$°C), which served as a reference for AES analysis by a 20 ML thick Ge cap layer at room temperature, the substrate temperature was increased in steps of about 100°C, while the LEED pattern was observed simultaniously. The time between subsequent annealing steps was 10 min. At $T_s = 500$°C weak LEED spots appear which become more intense in the course of the annealing interval. However, very similar to the LEED patterns which have been obtained when carrying out the Sn segregation experiments (subsection 3.1), at $T_s > 400$°C additional spots characteristic of island formation and facetting are observed. The formation of extended white areas which are irregularily distributed over the sample surface can again be explained by Sn segregation and clustering. The Ge diamond crystal lattice is obviously no longer able to stabilize these clusters and a recrystallization into the metalic β-phase takes place. This is further confirmed by the occurrence of a strong I_{Sn}/I_{Ge} AES signal, as indicated in fig. 5, which corresponds to a homogeneous Sn coverage of about 2 ML. From these results it is evident that solid phase epitaxy is not capable of producing single-crystal superlattices based on Ge and Sn.

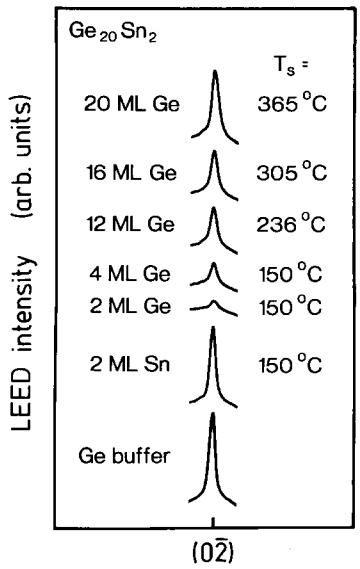

Fig. 8. Evolution of the (0$\bar{2}$) LEED intensity ($E_e = 182$ eV) within the first period of a $Ge_{20}Sn_2$ SL structure deposited at $150 < T_s < 365$°C.

In order to investigate the structural uniformity of the layers, which has been achieved by the described substrate modulation technique, cross-sectional TEM was performed on the two most promising superlattice samples, i.e. the structures which have been grown in the temperature intervals of $50 < T_s < 230$°C and $150 < T_s < 365$°C, respectively. Fig. 9 – bright field images in [110] projection with the (004) reflection strongly excited – compares these SLs. For the $Ge_{20}Sn_2$ superlattice deposited at the lower substrate temperatures, clearly distinguishable dark and bright lines, which correspond roughly to the Sn and Ge layers, can be observed throughout the whole structure with an overall thickness of 20 periods (Fig. 9a). In contrast, the layering of the 12-period SL shown in fig. 9b, which was grown at $150 < T_s < 365$°C, is very wavy and planar growth occurs only within the first period. Additional information on the lattice construction as well as on the concentration profiles within the SLs was obtained by means of high-resolution TEM. In the lattice image of the 20-period structure ($50 < T_s < 230$°C) depicted in fig. 10, the Sn-rich regions appear as dark bands. Since the electron beam is exactly [110] oriented, either the dark or bright dots correspond to atom pairs with the projection of their axes pointing in the [001] direction [34]. Thus, 11 dots should appear in growth direction for the 22 atomic monolayer periodicity which is indeed observed as indicated. Although the interfaces are smeared out – particularly in the growth direction as expected from AES analysis – the lattice construction is nearly perfect and no appreciable crystal defect could be detected over the whole area transparent to the electron beam (≈ 50 μm). This directly demonstrates the pseudomorphic nature of growth. In the SAD pattern of the sample shown in fig. 11, sharp superlattice spots appear due to the artificial periodicity along the growth direction. Since the area selected by the SAD aperture includes also Ge substrate

regions this diffraction pattern is a superposition of diffraction spots originating from the Ge substrate and the $Ge_{20}Sn_2$ SL. Besides the superlattice periodicity, therefore, both the lateral lattice constant and the average lattice constant in growth direction of the SL can be determined with an accuracy of about 0.5% relative to the substrate [29,35]. We note here that since the SL is lattice matched to the Ge substrate there is no deviation between the rows of superlattice spots and Ge bulk spots in the lateral direction.

A more accurate method to measure the period length of short-period superlattices is X-ray diffraction. From the θ–2θ satellite spacing (fig. 12), we extract a superlattice period of 31.85 ± 0.05 Å for $Ge_{20}Sn_2$, which is consistent with the value obtained from SAD analysis. This is in excellent agreement with the theoretical value of 31.89 Å for the structure calculated under the assumption of tetragonal deformation of the strained Sn layers expressed by macroscopic elasticity theory (see appendix).

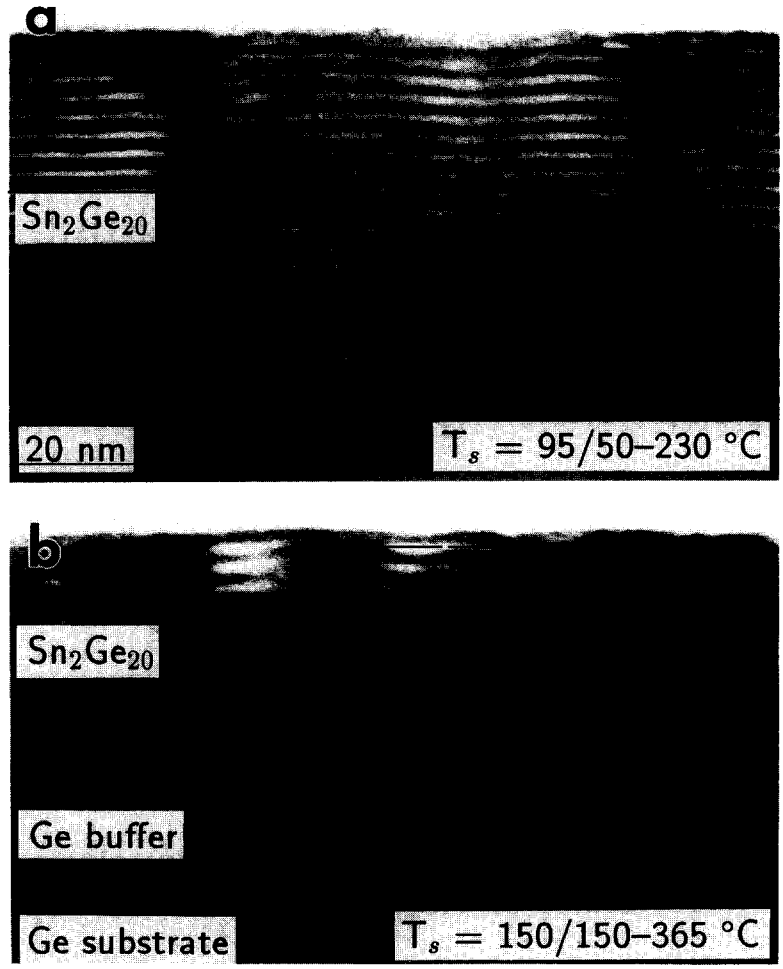

Fig. 9. Cross-sectional TEM bright field images (g = (004)) of $Ge_{20}Sn_2$ SLs with an overall thickness of (a) 20 and (b) 12 periods. The electron beam has been aligned close to the [110] direction parallel to the interfaces. The indicated substrate temperatures correspond to Sn and Ge deposition, respectively (see fig. 5).

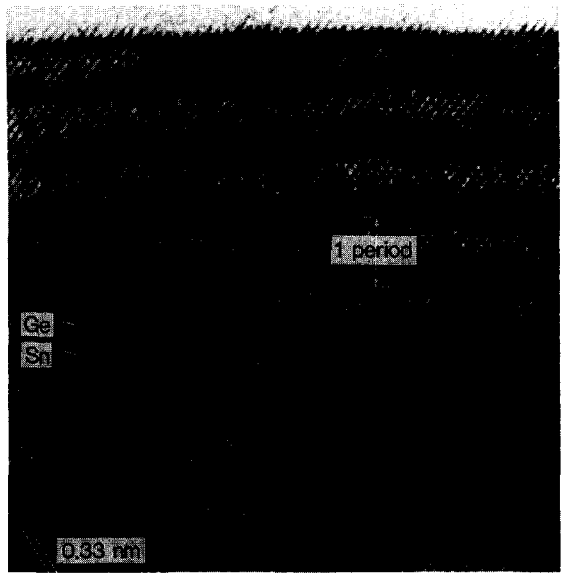

Fig. 10. High-resolution lattice image of the $Ge_{20}Sn_2$ SL which has been deposited at $50 < T_s < 230$°C taken along the [110] axis.

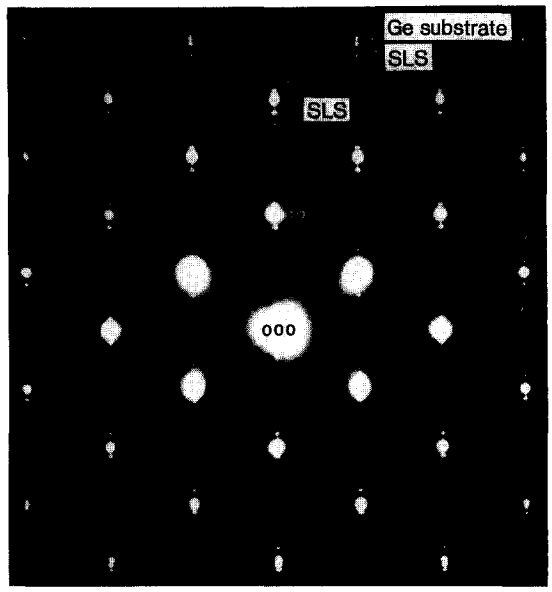

Fig. 11. SAD pattern of the 20-period $Ge_{20}Sn_2$ SL shown in figs. 9a and 10 in the [110] pole. Superlattice induced satellites (labelled SLS) in the vicinity of the Ge(004) reflection are marked by arrows. Note the splitting between higher order SL and Ge substrate reflections and the coincidence of superlattice and substrate spot rows in lateral direction.

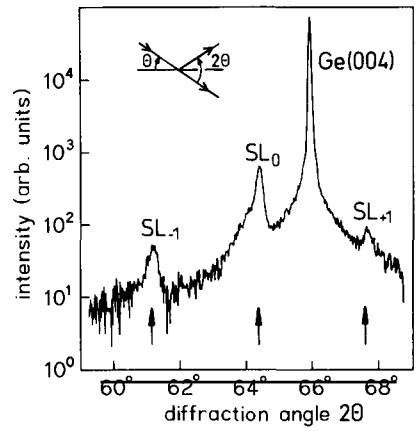

Fig. 12. X-ray diffraction from the 20-period $Ge_{20}Sn_2$ SL shown in figs. 9a and 10 in the vicinity of the Ge(004) reflection. The arrows mark the positions of the SL satellites for the expected period length of 31.89 Å.

Although substrate temperature modulation assisted MBE is clearly not able to produce Ge/α-Sn SLs with atomically abrupt interfaces as in the case of heterostructures based on Si and Ge [32,35], these results confirm that by careful choice of the growth parameters the application of this technique leads to single-crystal films with Sn contents far in excess of those achievable by $Ge_{1-x}Sn_x$ alloy growth using conventional MBE. However, since successful growth has only been demonstrated for one specific superlattice type ($Ge_{20}Sn_2$), further limitations in structural design of Ge_nSn_m SLs, i.e. the maximum achievable Sn layer thickness m and the minimum period length $n + m$, have to be expected. For this purpose two sets of superlattice samples with (i) a fixed period length of $n + m = 22$ ML and different SD layer thicknesses and with (ii) periodicities of $n + m =$ 22, 16, 12 and 10 ML and and constant Sn layer thickness of $m = 1$ ML have been prepared.

Fig. 13 compares the LEED patterns recorded after growth of the second period of the samples containing 1, 2 and 3 ML Sn within one 22 ML superlattice period. Although almost identical substrate temperature modulations have been performed during deposition of the the three structures, a dramatic decrease of the spot intensities accompanied by a strong increase in background intensity can be observed as the Sn layer

thickness exceeds 2 ML. Since this effect occurs also for SLs with doubled period length ($n + m$ = 44 ML) we conclude that the critical thickness for two-dimensional growth of epitaxially stabilized α-Sn on Ge(001) is 2 ML. Larger Sn layer thicknesses lead obviously to increased surface roughness which then supports the transition to amorphous Ge growth. No substantial improvement of the crystal quality can be detected by LEED when reducing the Sn layer thickness to 1 ML (fig. 13). However, the appearance of Pendellösung fringes in the high-resolution X-ray diffraction spectrum of the $Ge_{21}Sn_1$ SL shown in fig. 14a, which can be reproduced by a simulation which takes dynamical diffraction effects into account (fig. 14b), demonstrated the high crystalline

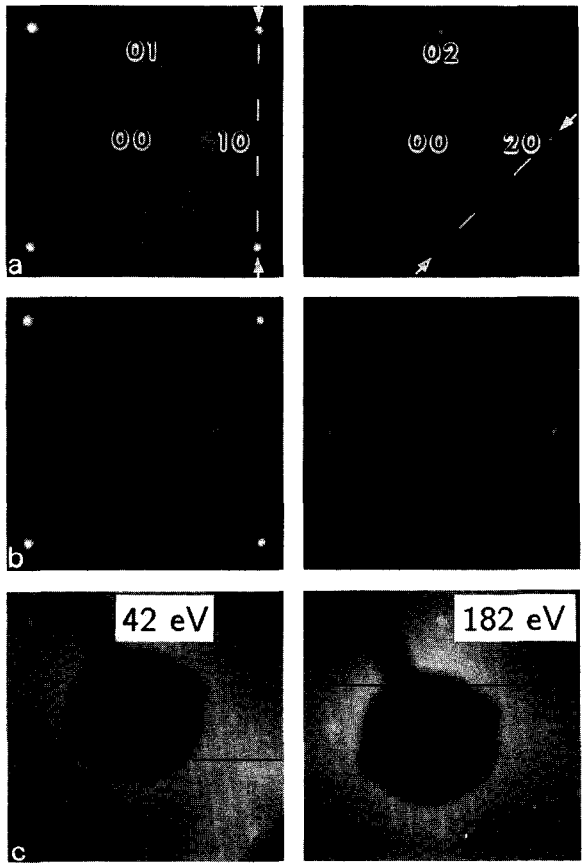

Fig. 13. LEED patterns (E_e = 42 and 182 eV) recorded after deposition of the second period of $Ge_{22-n}Sn_n$ SLs: (a) $Ge_{21}Sn_1$; (b) $Ge_{20}Sn_2$; (c) $Ge_{19}Sn_3$.

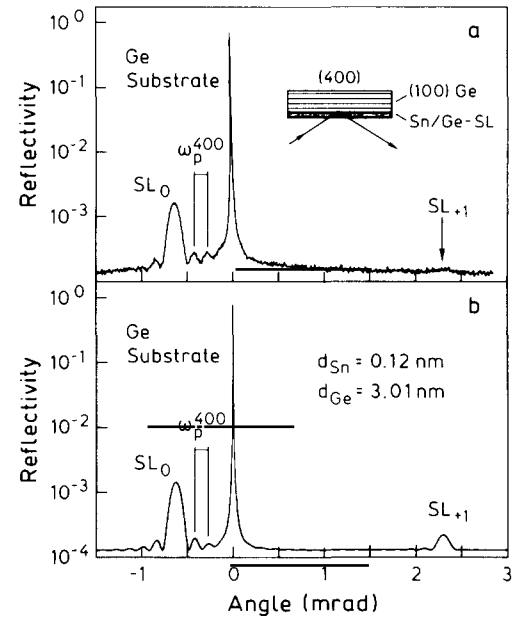

Fig. 14. High-resolution X-ray diffraction from the (400) reflection of a 20-period $Ge_{21}Sn_1$ SL (a) and corresponding simulation (b). The periodicity of Pendellösung fringes is indicated.

perfection of this sample. Results on a detailed characterization of the Ge/α-Sn SLs with this technique using both symmetric and asymmetric reflection geometry will be presented elsewhere [36].

In the LEED patterns of the second sample set which consists of 20-period SLs with period lengths ranging from 22 to 10 ML intense diffraction spots are observable for all structures throughout the whole superlattice growth. However, as the superlattice periodicity is reduced, spot broadening, in particular for the $Ge_{11}Sn_1$ and Ge_9Sn_1 SLs, occurs after completion of the 20th period. For these two structures the maximum substrate temperatures which were reached at the end of the Ge layers had to be increased to 265 and 300°C, respectively, in order to preserve crystalline growth. However, even for these high substrate temperatures where segregation induced interfacial intermixing is enhanced and for a Sn layer thickness of only 1 ML, the individual superlattice layers are planar and can be clearly

distinguished in TEM cross-sections, as demonstrated in fig. 15 for the shortest-period structure.

Additional information on composition and period length of the Ge_nSn_1 SLs can be also extracted from the Raman scattering data shown in fig. 16. The peak at 304 cm^{-1} which can be attributed to the Ge longitudinal phonon of the unperturbed Ge layers, is the prominent feature in all spectra. So-called folded longitudinal acoustical (LA) phonons [37], which appear in the frequency range below 150 cm^{-1} confirm the artificial superperiodicity of our structures. These are caused by backfolding of the acoustic phonon branch due to the superlattice induced reduction of the Brillouin zone. Therefore, the energetic positions of the LA modes depend critically on the superlattice period. In the inset of fig. 16, the wave numbers of the first ($|m| = 1$) and second

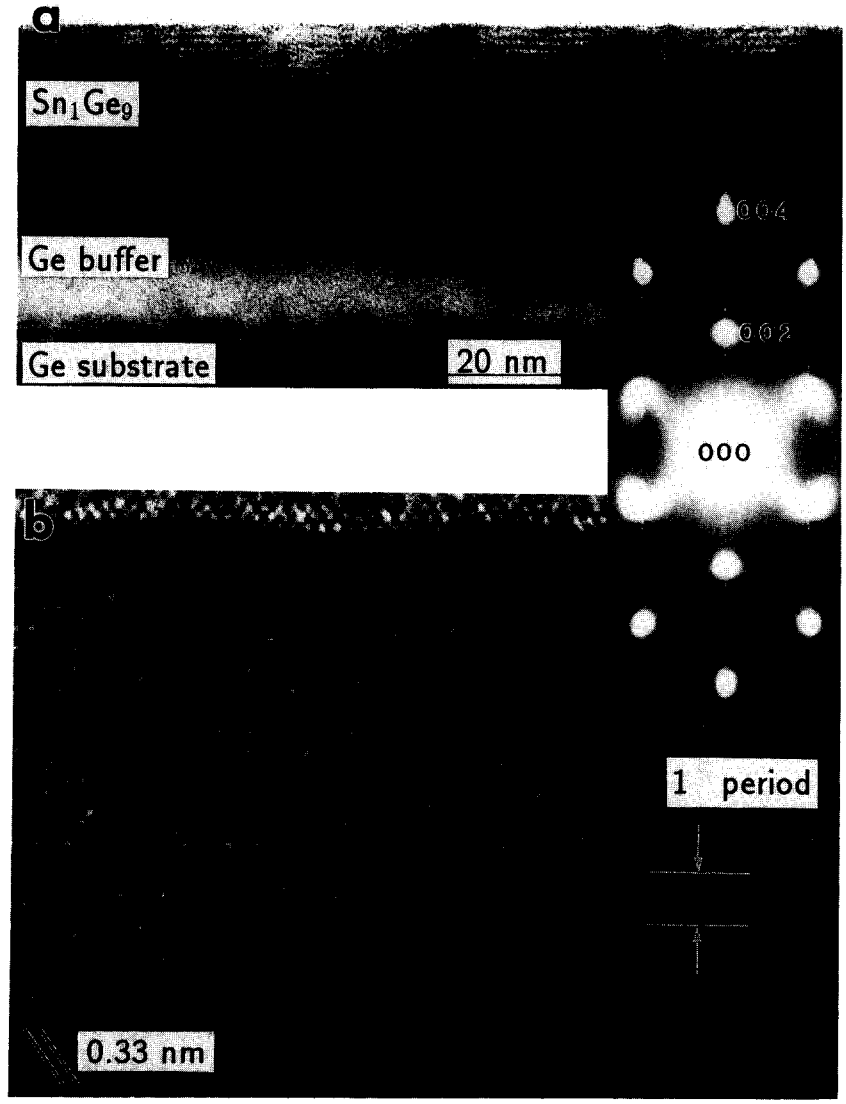

Fig. 15. TEM cross-sections of a 20-period Ge_9Sn_1 SL: (a) bright field image with the (004) reflection strongly excited and (b) high-resolution lattice image in [110] projection. Inset: SAD pattern of the superlattice taken in the [110] zone axis.

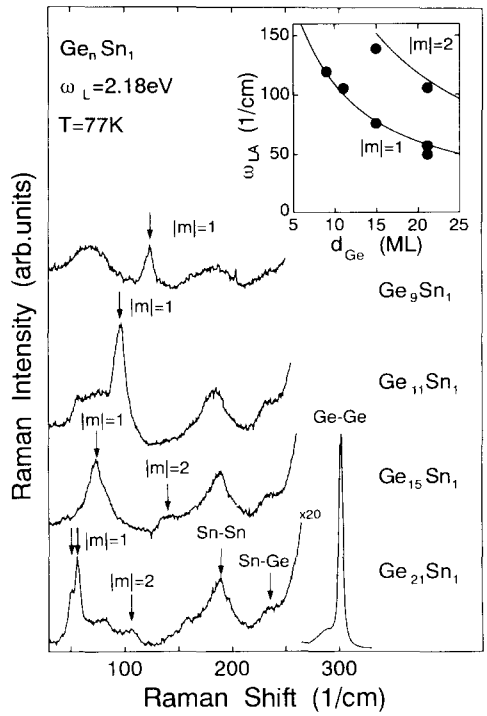

Fig. 16. Raman spectra of four Ge_nSn_1 SLs with an overall thickness of 20 periods. The inset compares the calculated energies of the folded acoustic modes (lines) with the experimentally determined energies (filled circles).

($|m| = 2$) order LA phonons, calculated within an elastic continuum model [37] which assumes an averaged sound velocity, are plotted versus the Ge layer thickness. Comparison with the experimentally determined phonon energies reveals excellent agreement for the $|m| = 1$ and reasonable agreement with the $|m| = 2$ modes for which the assumed linear dispersion of the acoustic phonon branch is not justified.

Due to the significant intermixing of the Sn and Ge layers also Sn–Sn, Sn–Ge and Ge–Ge vibrations in $Ge_{1-x}Sn_x$ alloy regions should be observable. The peak at about 180 cm^{-1}, which is clearly different from second order Raman scattering in Ge [38], can be attributed to Sn–Sn vibrations. This mode is shifted downwards compared to the α-Sn optical phonon which is expected at 200 cm^{-1} [39]. In the Raman spectra of the $Ge_{21}Sn_1$, $Ge_{15}Sn_1$ and $Ge_{11}Sn_1$ SLs, and weak structure can also be observed at about 230 cm^{-1}, which is believed to originate from Sn–Ge vibrations. Accordingly, the low-energy shoulder of the Ge optical phonon peak can be explained by Ge–Ge vibrations in the $Ge_{1-x}Sn_x$ alloy regions. The downward shift of the Sn–Sn Raman frequencies is in contradiction to recent experiments by Menéndez et al. [40], who studied relaxed $Ge_{1-x}Sn_x$ alloy layers ($0.92 < x < 0.98$) grown on CdTe(001). Our findings agree, however, with the behaviour in $Si_{1-x}Ge_x$ alloys where also a softening of the optical modes is observed. An unambiguous interpretation of the peaks at 180 and 230 cm^{-1} is not presently available, since disor-

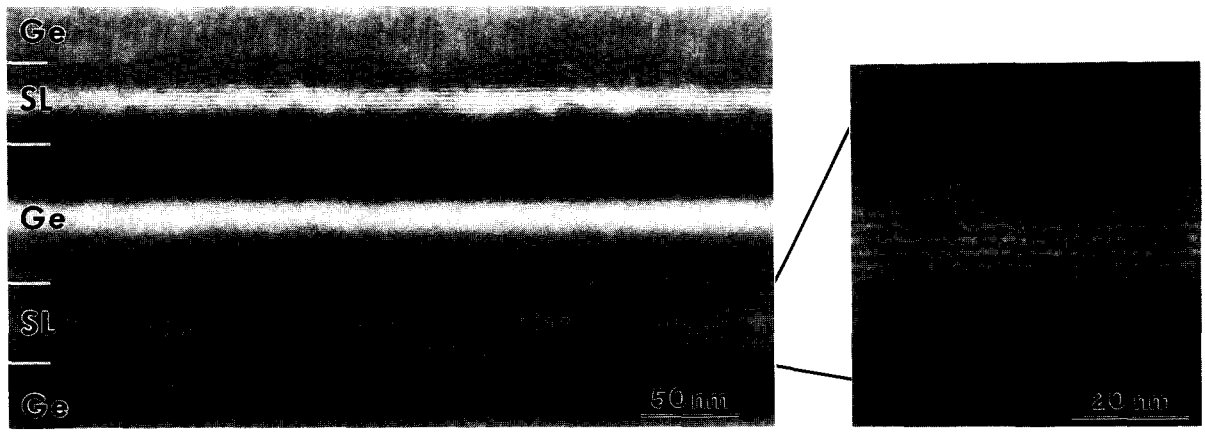

Fig. 17. Cross-sectional TEM bright-field image ($g = (004)$) of the sample containing four 20-period $Ge_{15}Sn_1$ SLs. The oscillatory contrast is due to interference of the electron waves transmitted through the wedge shaped TEM specimen (thickness fringes).

der activated modes originating in the Ge layers are also present in this energy region. A detailed Raman study employing polarization dependent measurements at different incident wavelengths is under way.

The additional broad structure at about 75 cm^{-1} observed in the spectra of the $Ge_{11}Sn_1$ and Ge_9Sn_1 SLs is propably caused by violation of wave vector conservation due to lattice disorder which gives rise to LA phonon scattering with large wave vectors. This confirms the LEED results which indicated already the onset of loss of crystalline order during growth of these structures. In contrast to the maximum achievable Sn layer thickness of Ge/α-Sn SLs pseudomorphic to Ge(001), it is, however, not possible to accurately determine the lower limit for the period length since the crystal quality of the structures degrades gradually as the periodicity is reduced.

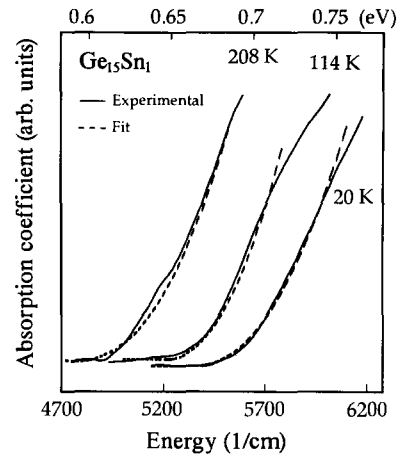

Fig. 18. Experimentally determined onset of absorption (full curves) in the $Ge_{15}Sn_1$ superlattice structure shown in fig. 17 for various temperatures. The dashed curves were obtained by fitting the band gap energy in the theoretical expression for the absorption of an ideal indirect semiconductor.

3.3.2. Band structure and optical properties

In order to obtain information on the fundamental band gap of the Ge/α-Sn heterostructures by infrared optical absorption measurements, samples with four superlattice sequences, each consisting of 20 periods with 700 Å thick Ge layers in between have been prepared. The purpose of the Ge layers is to decrease the average lattice mismatch $|f|$ of the whole structure relative to the Ge substrate while the effective thickness of the absorbing layer can be increased. Fig. 17 shows a cross-sectional bright field TEM image of the sample containing four $Ge_{15}Sn_1$ SLs. Although the initially planar layering becomes slightly wavy at the end of the twenty periods, a smooth starting surface for the next superlattice is regained by growth of the intermediate Ge layers at a substrate temperature of 310°C. In addition to the superlattice samples, we have grown under similar conditions a 2000 Å thick Ge layer on Ge(001) which served as a reference for the absorption measurements.

The absorption coefficient $\alpha(\hbar\omega)$ of the superlattice layers on Ge substrate can be calculated from the transmitted intensity through the whole structure $I(\hbar\omega)$ provided that the intensity $I_{ref}(\hbar\omega)$ transmitted through the reference sample is known. In order to achieve exactly the same conditions when determining these quantities, both the superlattice and the reference sample were mounted in the cryostat and measured using identical angles between the sample surface and the incident light. For small absorbance in the thin layers with an overall thickness d ($\alpha d < 1\%$) and for photon energies below the indirect band gap of the Ge substrate (0.76 eV at 20 K), the absorption coefficient is given by $\alpha = -(1/d)\ln(I/I_{ref})$, provided that I and I_{ref} are measured under normal incidence. Fig. 18 shows the absorption coefficient determined in this way for the $Ge_{15}Sn_1$ superlattice sample as a function of the photon energy for 20, 114 and 208 K. Good agreement is obtained with the photocurrent data of band to band transitions in these structures which have been recently presented by Olajos et al. [27]. Details of the absorption measurements are published elsewhere [41].

Assuming an ideal indirect semiconductor with quadratic dependence of α on energy near the absorption edge both for phonon absorption and emission processes [42], the band gap energies can be extracted from these data. Best numerical fits have been obtained for the dashed curves included in fig. 18. The deviation from the experimental curve at higher energies is due to the

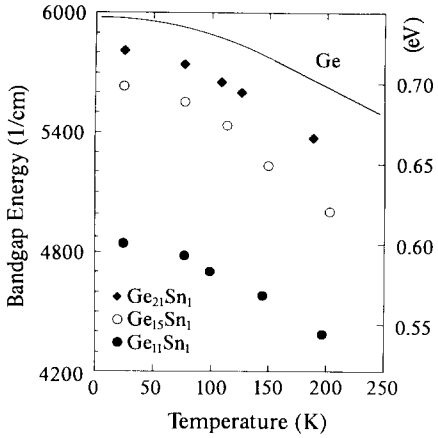

Fig. 19. Temperature dependence of the energy gap of Ge_nSn_1 SLs as extracted from the absorption measurements. For comparison the corresponding data of the indirect energy gap in bulk Ge (E_{Ge}^{ind}) are also included.

onset of the Ge band gap. Fig. 19 summarizes the results for the energy gaps of various Ge/α-Sn SLs in the temperature range of 20 to about 200 K. The temperature dependence of the indirect band gap in Ge is also indicated. All samples exhibit a typical initially quadratic and for higher temperatures linear decrease of the band gap with increasing temperature which is similar to the behaviour of pure Ge. However, as the average Sn concentration in the superlattices increases, a systematic lowering of the energy gap can be observed. The experimental values for 20 K of 0.6 eV ($Ge_{11}Sn_1$), 0.7 eV ($Ge_{15}Sn_1$) and 0.72 eV ($Ge_{21}Sn_1$) agree very well with those obtained from pseudopotential band structure calculations (0.63, 0.66 and 0.68 eV) performed by Vogl et al. [43]. To account for the interface broadening, the calculations have been performed within the virtual crystal approximation (VCA), assuming a Sn content of approximately 30% in the first atomic plane of the superlattice periods, followed by an exponential decay and a negligible concentration of Sn beyond a coverage of 10 ML. This concentration profile is based on the AES measurements which were carried out during deposition of the $Ge_{20}Sn_2$ at substrate temperatures of 50–230°C.

3.3.3. Structural stability against strain relaxation and phase transformation

In addition to the energy gaps of Ge_nSn_1 SLs (n = 11, 15 and 21) given in fig. 19, we attempted also to explore the band structure of a $Ge_{20}Sn_2$ SL. Although individual 20-period $Ge_{20}Sn_2$ SLs can be prepared almost defect-free (see subsection 3.3.1) structures consisting of four SLs seperated by 700 Å thick Ge layers have a high defect density as shown in fig. 20. Since the total thickness of each superlattice is about 640 Å, which

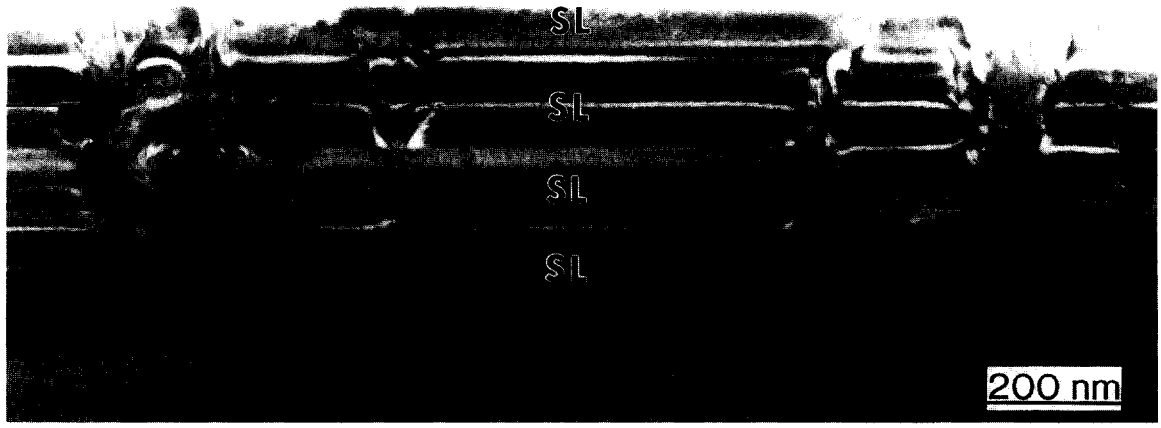

Fig. 20. Cross-sectional TEM bright-field image (g = (004)) of a strain relaxed sample containing four 20-period $Ge_{20}Sn_2$ SLs.

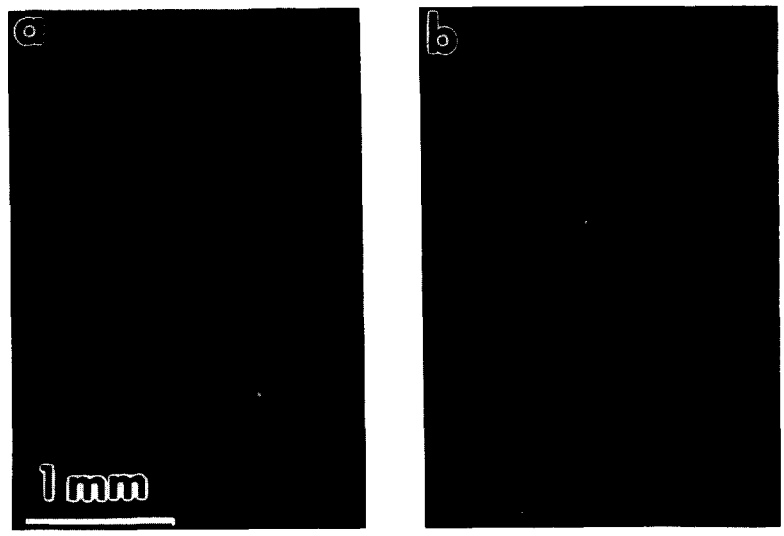

Fig. 21. Optical micrograph of the surface morphology of Ge/α – Sn SLs before (a) and after heat treatment (b).

exceeds the critical value for the misfit of $f \approx -1.4\%$ in this case by one order of magnitude (see appendix), these defects are obviously created due to strain relaxation of the whole structure. The catastrophic nature of the defects emphasizes the necessity to carefully design metastable Ge/α – Sn heterostructures with regard to the maximum achievable layer thicknesses given by the equilibrium theory.

As already mentioned in subsection 3.1, exceeding a substrate temperature of about 400°C when depositing Ge on Sn is accompanied by a distinct change in surface morphology, which has been ascribed to the $\alpha \rightarrow \beta$ phase transformation. A similar change in surface morphology has been reported by Piao et al. [44] for $Ge_{1-x}Sn_x$ alloy layers lattice matched to (001) oriented InP and GaSb substrates after heat treatment. In order to judge the thermal stability of our superlattice structures the samples have been annealed under vacuum conditions, while their surfaces were observed under a microscope. At a certain temperature, the mirror-like flat surface changes abruptly into a spotty surface. An example is shown in fig. 21. The $\alpha \rightarrow \beta$ phase transformation temperature depends, however, on the average Sn content in the SLs. Whereas the $Ge_{21}Sn_1$ superlattice structure is found to be stable for temperatures below 465°C, the transition temperatures of the $Ge_{15}Sn_1$ and the $Ge_{11}Sn_1$ SLs decrease to values of 450 and 430°C, respectively.

4. Conclusions and prospects

We have shown that the requirements for single crystal $Ge_{1-x}Sn_x$ alloy growth with $x \geq 0.1$ on Ge(001) substrates are incompatible with conventional MBE. This is mainly due to the extremely low Sn incorporation rates of less than 0.005 ML^{-1} at substrate temperatures of about 250°C which represent the lower limit for crystalline growth. In contrast, Ge/α-Sn superlattice layers with excellent crystal quality have been fabricated pseudomorphic to Ge(001) by means of an MBE technique which allows rapid variations of the substrate temperature during growth. Direct experimental evidence for absorption in these layers below the indirect band gap in Ge was presented. The fundamental energy gap of a series of Ge_nSn_1 SLs ($n = 21$, 15 and 11 ML) was found to decrease systematically with increasing Sn content confirming theoretical predictions based on pseudopotential band structure calculations for these structures. The introduction of such superlattice layers in the intrinsic regions of p–i–n

diodes offers the possibility of increasing the range of conventional Ge photodetectors to longer wavelengths. The limited thickness of the pseudomorphic structures could be easily overcome by alternating growth of undercritical Ge/α-Sn superlattice and Si_xGe_{1-x} alloy layers. Besides the critical thickness, the major limitation in structural design of single crystal Ge_nSn_m SLs was found to be the maximum achievable Sn layer thickness of $m = 2$ ML. Although for periodicities of $n + m \leq 12$ ML and average Sn concentrations exceeding a value of 10% a decay of crystalline order has been observed, these limitations are not fundamental and can be probably overcome by further optimizing the deposition technique. In this context, sample heating from the surface by halogen lamps as commonly used in rapid thermal chemical vapour deposition (RTCVD) systems could be considered.

According to the present theory, the fundamental band gap of Ge/α-Sn superlattices pseudomorphic to Ge(001) is always indirect in $\boldsymbol{k}$ space even for average Sn contents larger than 20% [26,27,43]. However, also the possibility of an intrinsic direct semiconductor is predicted, provided that the lateral lattice constant $a_{\parallel}$ of the Ge/α-Sn SLs is slightly increased with respect to a_{Ge}. Analogously to the Si/Ge system, this could be achieved in principle by growth of strain relaxed Ge/α-Sn alloy or superlattice layers. A different approach in order to verify these predictions would be to optimize MBE growth conditions, using materials such as InP as the substrate.

Acknowledgements

It is a pleasure to acknowledge the excellent collaboration with P. Vogl (TU München) who has carried out the band structure calculations and with H. Cerva and H. Oppolzer from the TEM group at Siemens Research Laboratories. We are also grateful to R. Zaus, H. Göbel (Siemens Research Laboratories) and L. Tapfer (CNRSM Mesagne) for performing the X-ray diffraction measurements. This work was supported financially by the Siemens AG via SFE "Mikrostrukturierte Bauelemente".

Appendix

In this appendix the strained $Ge_{1-x}Sn_x$ layers are assumed to be isotropic. In order to obtain the appropriate values for the alloy, the elastic constants C_{11} and C_{12} of Ge and α − Sn given below have been linearily interpolated.

For Ge:

$C_{11} = 1.315 \times 10^{11}$ N/m^2,

$C_{12} = 4.94 \times 10^{10}$ N/m^2;

For α-Sn:

$C_{11} = 6.9 \times 10^{10}$ N/m^2,

$C_{12} = 2.93 \times 10^{10}$ N/m^2.

Critical thickness for coherent growth

The critical thickness h_c at which it becomes energetically favourable to introduce the first misfit dislocation in a strained film can be calculated by minimizing the sum consisting of the elastic strain energy and the dislocation line energy [20], as well as by balancing the forces which act on a threading dislocation segment [21]. This leads to the following expression for the variation of h_c with $|f|$:

$$h_c = \frac{b(1 - \nu \cos^2\beta)}{8\pi |f| (1+\nu) \sin\beta \cos\theta} \ln\left(\frac{\alpha h_c}{b}\right), \qquad (1)$$

where b is the Burgers vector, ν is Poisson's ratio given by $C_{12}/(C_{11} + C_{12})$ within isotropic elasticity theory, β is the angle between $\boldsymbol{b}$ and the dislocation line, θ is the angle between the glide plane of the dislocation and the interface, and α is the core-energy parameter which is commonly taken to $\alpha = 4$ for covalently bonded semiconductors. In the calculation we assumed the formation of 60° (a/2)⟨110⟩ misfit dislocations on {111}

glide planes ($b \approx 4$ Å and $\cos\beta = \sin\beta \cos\theta = 0.5$).

Tetragonal deformation

The in-plane strain $\epsilon_{\|}$ in a $Ge_{1-x}Sn_x$ film pseudomorphic to Ge substrate is simply given by the misfit f between the two materials:

$$\epsilon_{\|} = f = (a_s - a_f)/a_f. \quad (2)$$

For (001) biaxial strain the perpendicular out of plane strain is related to $\epsilon_{\|}$ by [45]:

$$\epsilon_{\perp} = -\frac{2C_{12}}{C_{11}}\epsilon_{\|}. \quad (3)$$

Accordingly, the lattice constant perpendicular to the interface of the tetragonally deformed material is

$$a_{\perp} = a_f(1+\epsilon_{\perp}) = a_f\left[1 - \frac{2C_{12}}{C_{11}}\left(\frac{a_s}{a_f} - 1\right)\right]. \quad (4)$$

For pure totally strained α-Sn layers ($a_f = 6.489$ Å) a value of $a_{\perp} = 7.195$ Å is obtained, which corresponds to a thickness of one atomic layer of 1.799 Å.

References

[1] U. Gnutzmann and K. Clausecker, Appl. Phys. 3 (1974) 9.
[2] T.P. Pearsall, J. Bevk, L. Feldman, J.M. Bonar and J.P. Mannaerts, Phys. Rev. Letters 58 (1986) 729.
[3] R. Zachai, K. Eberl, G. Abstreiter, E. Kasper and H. Kibbel, Phys. Rev. Letters 64 (1990) 1055.
[4] M.S. Hybertsen and M. Schlüter, Phys. Rev. B 36 (1987) 9683.
[5] S. Froyen, D.M. Wood and A. Zunger, Phys. Rev. B 36 (1987) 4547; B 37 (1988) 6893.
[6] M.A. Gell, Phys. Rev. B 38 (1988) 7535; B 40 (1989) 1966.
[7] S. Groves and W. Paul, Phys. Rev. Letters 11 (1963) 194.
[8] D.W. Jenkins and J.D. Dow, Phys. Rev. B 36 (1987) 7994.
[9] K.A. Mäder, A. Baldereschi and H. von Känel, Solid State Commun. 69 (1989) 1123.
[10] C.H.L. Goodman, IEE Proc. 129 (1982) 189.
[11] G.A. Busch and R. Kern, in: Solid-State Physics, Vol. 11, Eds. H. Ehrenreich, F. Seitz and D. Turnbull (Academic Press, New York, 1961) p. 1.
[12] A.W. Ewald, J. Appl. Phys. 25 (1954) 1436.
[13] R.F.C. Farrow, D.S. Robertson, G.M. Williams, A.G. Cullis, G.R. Jones, I.M. Young and P.N.J. Dennis, J. Crystal Growth 54 (1981) 507.
[14] J.L. Reno and L.L. Stephenson, Appl. Phys. Letters 54 (1989) 2207.
[15] M.T. Asom, A.R. Kortan, L.C. Kimerling and R.C. Farrow, Appl. Phys. Letters 55 (1989) 1439.
[16] E.A. Fitzgerald, P.E. Freeland, M.T. Asom, W.P. Lowe, R.A. MacHarrie, Jr., B.E. Weir, A.R. Kortan, F.A. Thiel, Y.H. Xie, A.M. Sergent, S.L. Cooper, G.A. Thomas and L.C. Kimerling, J. Electron. Mater. 20 (1991) 489, and references therein.
[17] M.T. Asom, E.A. Fitzgerald, A.R. Kortan, B. Spear and L.C. Kimerling, Appl. Phys. Letters 55 (1989) 578.
[18] F.K. LeGoues, B.S. Meyerson and J.F. Morar, Phys. Rev. Letters 66 (1991) 2903.
[19] E.A. Fitzgerald, Y.H. Xie, M.L. Green, D. Brasen, A.R. Kortan, J. Michel, Y.J. Mii and B.E. Weir, Appl. Phys. Letters 59 (1991) 811.
[20] F.C. Frank and J.H. van der Merwe, Proc. Roy. Soc. (London) A 198 (1949) 205; A 198 (1949) 216; A 200 (1949) 125.
[21] J.W. Matthews and A.E. Blakeslee, J. Crystal Growth 27 (1974) 118; 29 (1975) 273; 32 (1976) 265.
[22] G. Abstreiter, K. Eberl, E. Friess, W. Wegscheider and R. Zachai, J. Crystal Growth 95 (1989) 431.
[23] H.-J. Gossmann, J. Appl. Phys. 68 (1990) 2791.
[24] P.R. Pukite, A. Harwit and S.S. Iyer, Appl. Phys. Letters 54 (1989) 2143.
[25] W. Wegscheider, K. Eberl, U. Menczigar and G. Abstreiter, Appl. Phys. Letters 57 (1990) 875.
[26] W. Wegscheider, K. Eberl, U. Menczigar, J. Olajos, G. Abstreiter and P. Vogl, in: Proc. 20th Intern. Conf. on the Physics of Semiconductors, Eds. E.M. Anastassakis and J.D. Joannopoulos (World Scientific, Singapore, 1990) p. 1685.
[27] J. Olajos, P. Vogl, W. Wegscheider and G. Abstreiter, Phys. Rev. Letters 67 (1991) 3164.
[28] M. Tabe, K. Arai and H. Nakamura, Japan. J. Appl. Phys. 20 (1981) 703.
[29] W. Wegscheider, K. Eberl, H. Cerva and H. Oppolzer, Appl. Phys. Letters 55 (1989) 448.
[30] S.S. Iyer, R.A. Metzger and F.G. Allen, in: Proc. 2nd Intern. Symp. on VLSI Science and Technology, Vol. 84-7 (Electrochemical Society, Pennington, NJ, 1984) pp. 473–487.
[31] J. Wilhelm, W. Wegscheider and G. Abstreiter, in: Proc. 5th Intern. Conf. on Modulated Semiconductor Structures, Nara, 1991, Ed. C.B. Duke [Surface Sci. 267 (1992) 90].
[32] K. Eberl, W. Wegscheider and G. Abstreiter, J. Crystal Growth 111 (1991) 882.
[33] H.P. Zeindl, T. Wegehaupt, I. Eisele, H. Oppolzer, H. Reisinger, G. Tempel and F. Koch, Appl. Phys. Letters 50 (1987) 1164.
[34] J.C.H. Spence, High-Resolution Electron Microscopy (Clarendon, Oxford, 1981) p. 166.

[35] G. Lütjering, W. Wegscheider, G. Abstreiter, H. Cerva and H. Oppolzer, unpublished.
[36] L. Tapfer, W. Wegscheider and G. Abstreiter, unpublished.
[37] B. Jusserand and M. Cardona, in: Light Scattering in Solids V, Topics in Applied Physics, Vol. 66 (Springer, Berlin, 1989) p. 49.
[38] M.A. Renucci, J.B. Renucci, R. Zeyher and M. Cardona, Phys. Rev. B 10 (1974) 4309.
[39] M. Iliev, M. Sinyukov and M. Cardona, Phys. Rev. B 16 (1977) 5350.
[40] J. Menéndez, K. Sinha, H. Höchst and M.A. Engelhardt, Appl. Phys. Letters 57 (1990) 380;
J. Menéndez, K. Sinha, H. Höchst and M.A. Engelhardt, in: Light Scattering in Semiconductor Structures and Superlattices, NATO–ASI Series, Eds. D.J. Lockwood and J.F. Young (Plenum, New York, 1991) p. 33.
[41] J. Olajos, W. Wegscheider and G. Abstreiter, submitted for publication.
[42] G.F. Bassani and G.P. Parravicini, Electronic States and Optical Transitions in Solids (Pergamon, Oxford, 1975).
[43] P. Vogl, J. Olajos, W. Wegscheider and G. Abstreiter, in: Proc. 5th Intern. Conf. on Modulated Semiconductor Structures, Nara, 1991, Ed. C.B. Duke [Surface Sci. 267 (1992) 83].
[44] J. Piao, R. Beresford, T. Licata and W.I. Wang, J. Vacuum Sci. Technol. B 8 (1990) 221.
[45] C.G. Van de Walle and R.M. Martin, Phys. Rev. B 34 (1986) 5621.